nature portfolio

https://doi.org/10.1038/s41551-021-00791-0

Supplementary information

Metabolic and immunomodulatory control of type 1 diabetes via orally delivered bile-acid-polymer nanocarriers of insulin or rapamycin

In the format provided by the authors and unedited

Contents

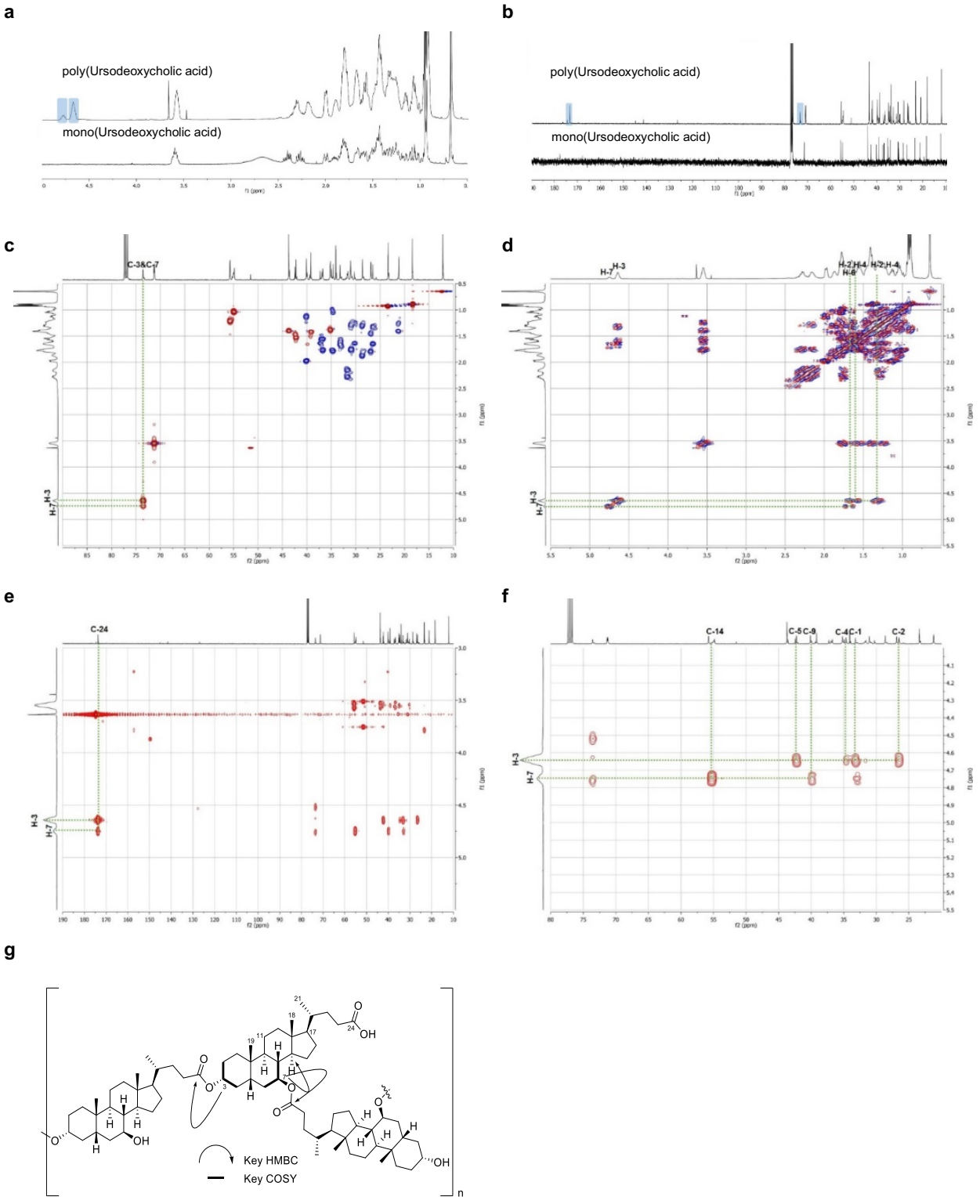

Supplementary Fig. 1. Polymerized UDCA and monomer characterization by nuclear magnetic resonance (NMR). a, Compared to the spectrum of UDCA, the ^{1}H NMR spectrum (600 MHz, chloroform-d_1) of polymerized UDCA revealed the presence of two additional methine proton signals (δ_H 4.75 and 4.64) in the range of oxygen-bearing proton chemical shifts. **b**, Similarly, the ^{13}C NMR spectral data (100 MHz, chloroform-d_1) of polymeric UDCA shows a shifted carbon signal attributable to ester carbon chemical shift (δ_C 170.7). It also shows a distinct oxygenated signal (δ_C 73.6), which confirms a biodegradable ester bond between monomeric units (highlighted in blue). Chemical structure of polymer bile acid (pBA) was further supported by the interpretation of two-dimensional [^{1}H-^{1}H double-quantum-filtered correlation spectroscopy (^{1}H-^{1}H DQF-COSY), ^{1}H-^{13}C heteronuclear single-quantum coherence (^{1}H-^{13}C HSQC), and ^{1}H-^{13}C heteronuclear multiple-bond correlation (^{1}H-^{13}C HMBC)] NMR spectra. One-dimensional NMR spectrum,

most commonly ^{1}H and ^{13}C, describes the signal intensity, existence and frequency of a single nucleus within the molecules. 2D NMR correlation spectrum describes correlations between nuclei in two different frequency axes (^{1}H and ^{1}H for COSY , or ^{1}H and ^{13}C for HSQC and HMBC). In the ^{1}H-^{1}H COSY spectrum, the diagonal peaks correspond to a 1D ^{1}H NMR spectrum and off-diagonal peaks correspond to couplings between protons and protons within the molecule. ^{1}H-^{13}C HSQC and ^{1}H-^{13}C HMBC NMR spectra show one bond and two-four bonds correlations between protons and carbons, respectively. **c**, Interpretation of the HSQC NMR spectral data coupled with ^{13}C NMR spectral data allowed us to assign two oxygenated methine protons at δ_H 4.75 and 4.64 to the directly bonded carbon (δ_C 73.6). Assignments of all of the data in **c** suggested the formation of two distinguishable ester groups at C-3 and C-7, respectively. **d**, The sequential ^{1}H-^{1}H DQF-COSY correlations from H-3 (δ_H 4.64) to H-2 and H-4, and from H-7 (δ_H 4.75) to H-6 and H-8 further supported the two ester groups are attached to C-3 and C-7. **e, f**, HMBC NMR spectra of polymeric UDCA. ^{1}H-^{13}C HMBC correlation from H-3 (δ_H 4.64) and H-7 (δ_H 4.75) to carbonyl ester group (δ_C 170.7), and from H-7 (δ_H 4.75) to a methine carbon C-9 (δ_C 55.2) unambiguously established the esterification of UDCA monomers to be polymerized at C-3 and C-7 in A-ring and B-ring, respectively. **g**, Bond correlations in pUDCA revealed by Key HMBC and COSY NMR spectra**.** Consistent with results shown in **c-f**, the structure of pUDCA can be understood as shown above. Given the intensities of ^{1}H NMR signals which provide information on the relative number of protons, NMR data of pUDCA revealed that two hydroxyl substituents at C-3 and C-7 were esterified with 2.5 : 1 molar ratio during the polymerization process.

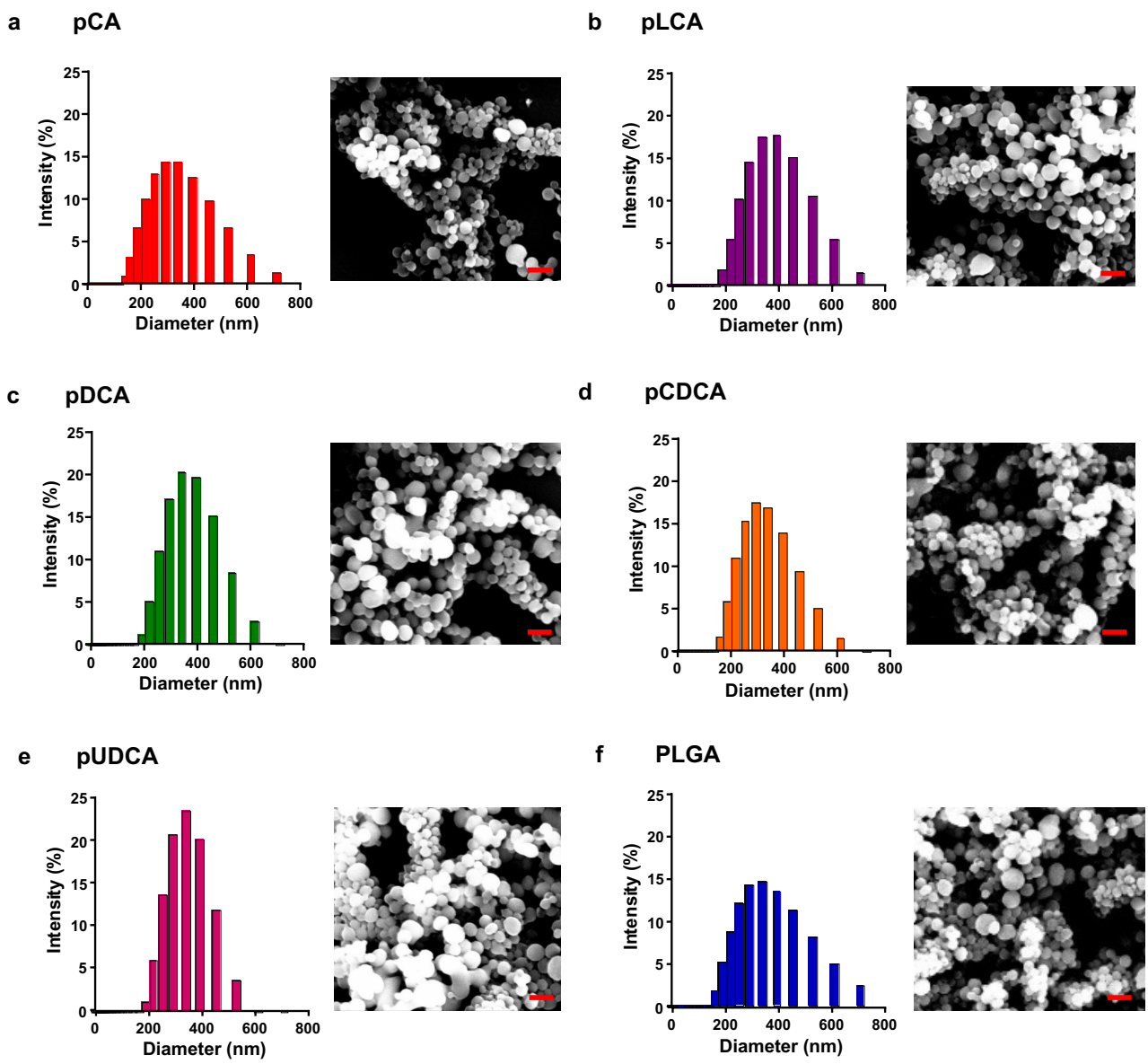

Supplementary Fig. 2. Assessment of nanoparticle size distribution and morphology. Nanoparticles (NPs) were fabricated using the W/O/W double emulsion method and the size was measured by dynamic light scattering (DLS, Zetasizer, Malvern Instruments). The size of NPs was well controlled (average dimeter: **a**, poly(cholic acid) (pCA) 360.3 ± 11.2 nm; **b**, poly(lithocholic acid) (pLCA) 337.9 ± 21.0 nm; **c**, poly(deoxycholic acid) (pDCA) 311.9 ± 24.1 nm; **d**, poly(chenodeoxycholic acid) (pCDCA) 335.1 ± 9.8 nm; **e**, poly(ursodeoxycholic acid) (pUDCA) 344.3 ± 4.7 nm; **f**, poly(lactic-co-glycolic acid) (PLGA) 328.8 ± 3.4 nm) in order to compare their *in vitro* cellular interaction and biodistribution independent on their size variation because particle size is critical in cellular uptake, intestinal transport, organ distribution, and body clearance. The spherical morphology of the NPs was observed by Hitachi S-4800 High Resolution scanning electron microscopy (SEM, Hitachi SU-70, Norcross) and the particle size in the images was in agreement with the results obtained by DLS. (Red size bars = 0.5 μm)

Supplementary Table 1: Molecular weight properties of bile acid polymers and physical/loading properties of nanoparticles fabricated from the polymers.

	Mn[a]	Mw[b]	PDI[c]	Mean diameter (nm)	PDI[d]	Zeta-potential (mV)	Dye loading (%)[e]	Loading efficiency (%)[f]
PLGA	2451	4184	1.707	328.8 ± 3.4	0.304	-27.5 ± 2.8	0.699 ± 0.045	69.9 ± 4.5
pCA	1972	2962	1.502	360.3 ± 11.2	0.296	-24.6 ± 3.1	0.702 ± 0.012	70.2 ± 1.2
pLCA	1357	1598	1.177	337.9 ± 21.0	0.276	-27.1 ± 10.4	0.730 ± 0.020	73.0 ± 2.0
pDCA	1842	2523	1.370	311.9 ± 24.1	0.213	-22.7 ± 1.5	0.687 ± 0.064	68.7 ± 6.4
pCDCA	1741	2284	1.312	335.1 ± 9.8	0.011	-27.8 ± 10.1	0.687 ± 0.014	68.7 ± 1.4
pUDCA	2225	3210	1.443	344.3 ± 4.7	0.164	-24.9 ± 4.4	0.674 ± 0.005	67.4 ± 0.5
Blend (pUDCA/ PLGA)[g]	-	-	-	299.5 ± 14.3	0.131	-22.2 ±5.6	0.726 ± 0.019	72.6 ± 1.9

[a] The number average molar mass (GPC)
[b] The weight average molar mass (GPC)
[c] Polymer polydispersity index (GPC)
[d] Particle polydispersity index (DLS)
[e] (weight of encapsulated dye / weight of NPs) × 100
[f] (weight of encapsulated dye / weight of dye used for encapsulation) × 100
[g] Polymer blend nanoparticles (pUDCA:PLGA=50:50, w/w).

Supplementary Table 2: Kinetic constants for internalization and exocytosis of nanoparticles.

	k_{exo} (1/h)	k_{endo} (mL/mg·h)
pUDCA	0.085	0.8137
PLGA/ pUDCA	0.040	0.5688
PLGA	0.023	0.3523

Supplementary Table 3: Fitting parameter (EC50) for impact of PUDCA avidity on TGR5 binding and insulin secretion compared to monomer UDCA.

a

#UDCA/NP	EC_{50}
pUDCA	42.2 ± 16.8
2000/NP	73.9 ± 15.1
1000/NP	87.6 ± 15.5
500/NP	100.3 ± 20.0
100/NP	113.5 ± 17.4
0/NP	N/A

b

#UDCA/NP	EC_{50}
pUDCA	189.1 ± 30.8
2000/NP	393.2 ± 39.9
1000/NP	387.7 ± 17.6
500/NP	503.7 ± 67.1
100/NP	469.3 ± 97.2
0/NP	N/A
Free dye	N/A

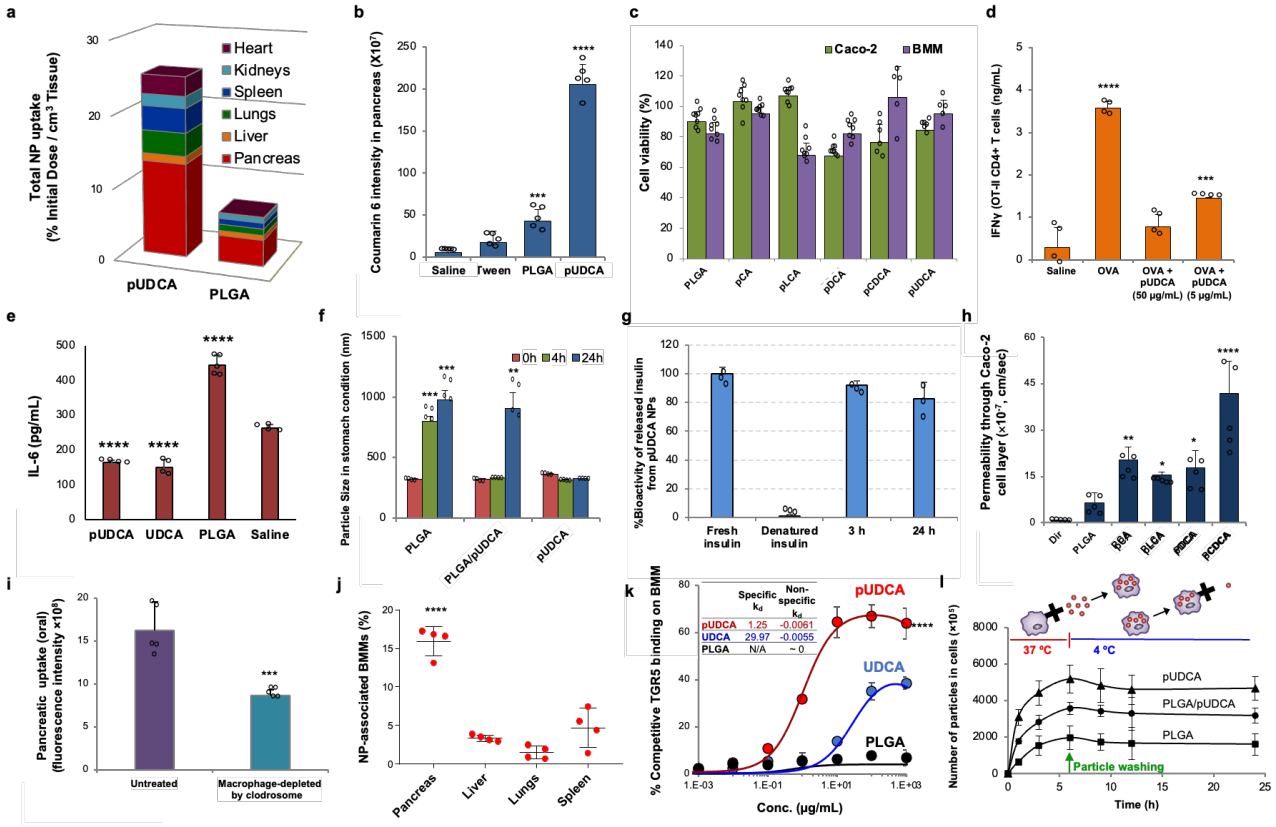

Supplementary Fig. 3. Properties of polymer bile acids (pBAs) *in vitro* and *in vivo*. Figures are presented in the order that is discussed in the main manuscript. **a**, Comparison between pUDCA and control PLGA NPs in the biodistribution in non-gastrointestinal organs (n=6). **b**, Dye-independent localization of NP in the pancreas (n=5, mean ± SD, one-way ANOVA to saline, $P_{PLGA} = 0.0009$, $P_{pUDCA} < 0.0001$). Pancreatic accumulation of NPs was quantitated when coumarin 6 was used as a tracer confirming that level of pancreatic accumulation of NP was independent of the physiochemical properties of the loaded agent, but dependent on the particle composition. Free coumarin was dispersed in 1% tween 20 in saline. **c**, Cytotoxicity of NPs (1 mg/mL) in Caco-2 cells (10^4 cells/well) and BMMs (10^4 cells/well) was measured using a CellTiter-Blue® Cell Viability Assay (Promega Co.) after incubation at 37°C for 24 h (n=8, mean ± SD). **d**, OT-II T cells were cocultured with pUDCA-treated dendritic cells (DCs) that were stimulated by lipopolysaccharide (LPS) and ovalbumin (OVA) (n=4, mean ± SD, one-way ANOVA to saline, $P_{OVA} < 0.0001$, $P_{pUDCA\ 5} = 0.0005$). Decrease in the interferon gamma (IFNγ) level from OT-II CD4+ T cells were measured. **e**, pUDCA impact on secretion of pro-inflammatory cytokine, IL-6, from macrophages (n=4-5, mean ± SD, one-way ANOVA to saline, $P_{pUDCA,\ UDCA,\ and\ PLGA} < 0.0001$). **f**, Particle stability was evaluated by measuring particle sizes over time in the simulated stomach conditions (citrate buffer solution, pepsin 10 mg/mL, pH 2.0, 37°C) (n=4, mean ± SD, two-way ANOVA to 0h, $P_{PLGA\ 4h} = 0.0003$, $P_{PLGA\ 24h} = 0.0008$, $P_{PLGA/pUDCA\ 24h} = 0.0052$). **g**, Bioactivity of released insulin from pUDCA. The released insulin from pUDCA at 3 or 24 h was incubated with CHO INSR cells for 1 h and pAkt was measured by ELISA. The pAkt production from CHO INSR cells that were incubated with fresh or denatured insulin was measured to calculate %bioactivity. The average bioactivity of released INS was 87.3% of fresh insulin (n=3, mean ± SD). **h**, Permeability of NPs through a layer of Caco-2 cells on transwell filters (n=5, mean ± SD, one-way ANOVA to Dir, $P_{pCA} = 0.0031$, $P_{pLCA} = 0.0367$, $P_{pDCA} = 0.0114$, $P_{pCDCA} < 0.0001$). **i**, Pancreatic trafficking with and without macrophage depletion. B6 mice were depleted macrophages and treated with DIR-loaded pUDCA NPs by oral gavage (500 mg/kg, 250 μL). Clodrosome (Clodronate-containing liposomes, 100 mg/kg, IP) was used to deplete macrophages. Pancreata were harvested at 4 h post gavage and imaged (n=5, mean ± SD, one-way ANOVA, P = 0.0005). **j**, CD11c-F4/80+ macrophages associated with coumarin 6-loaded pUDCA NPs in pancreas, liver, lungs, and spleen in mice were acquired using a flow cytometer at 4 h post oral ingestion (n=4, mean ± SD, one-way ANOVA to other organs, P < 0.0001). **k**, Competitive binding of pUDCA and UDCA to TGR5 on macrophages at 4°C (n=6, mean ± SD, one-way ANOVA to UDCA, $P_{pUDCA} < 0.0001$). **l**. Rate of endocytosis 37°C and exocytosis at 4°C (n=8, mean ± SD).

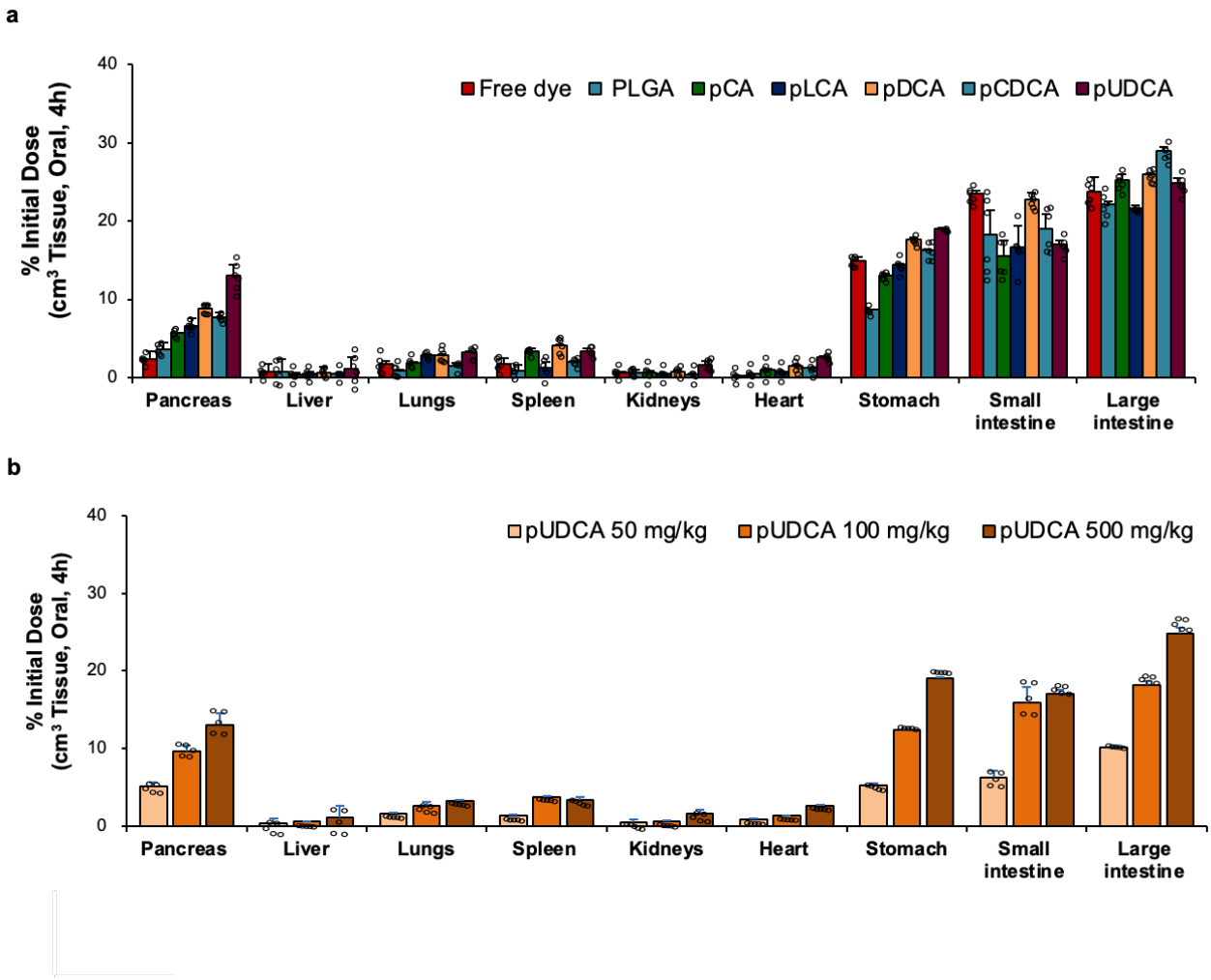

Supplementary Fig. 4. Organ distribution of polymer bile acid (pBA) NPs and dose dependency. a, Organ level biodistribution of orally ingested pBAs and control PLGA NPs as compared to free dye. Mice were fasted for 4 h then orally gavaged with DIR-encapsulating pBA NPs (500 mg/kg) (n=6, mean ± SD). **b**, Dose-dependent distribution of DIR-loaded pUDCA NPs was also investigated (oral gavage at 50, 100, and 500 mg/kg) (n=5, mean ± SD). The increased fluorescence levels at 4 h post NP ingestion was due to digestive kinetics in the stomach and intestines, and not steady state biodistribution accumulation.

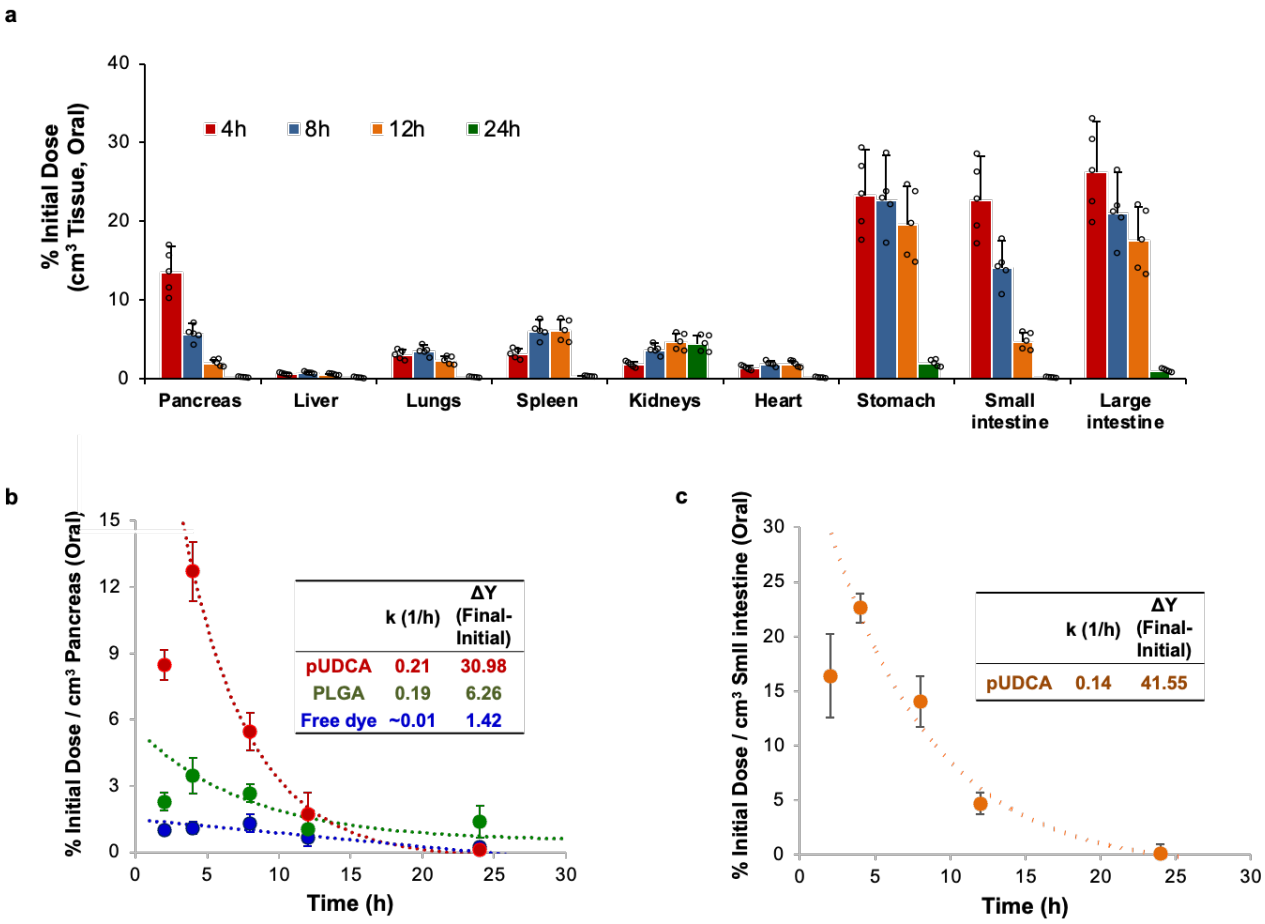

Supplementary Fig. 5. Accumulation and clearance of pUDCA NPs in pancreas and GI organs. a, NP uptake in organs was measured at time points of 4, 8, 12, and 24 h. Generally, peak uptake of pUDCA in organs at 4 h was found post oral gavage and the particles cleared after 24 h through kidneys (n=5, mean ± SD). **b, c**, Clearance rates (k) and ΔY (inset) from pancreas and small intestine was calculated by non-linear regression curve fitting (one phase decay). $Y=(Y_0 - \text{Plateau})\times\exp(-k\times t) + \text{Plateau}$, where Y_0 is the Y value when t (time) is zero. Plateau is the Y value at infinite times, k is the rate constant. pUDCA showed at least five fold greater pancreatic accumulation compared to controls and its clearance was similar to PLGA.

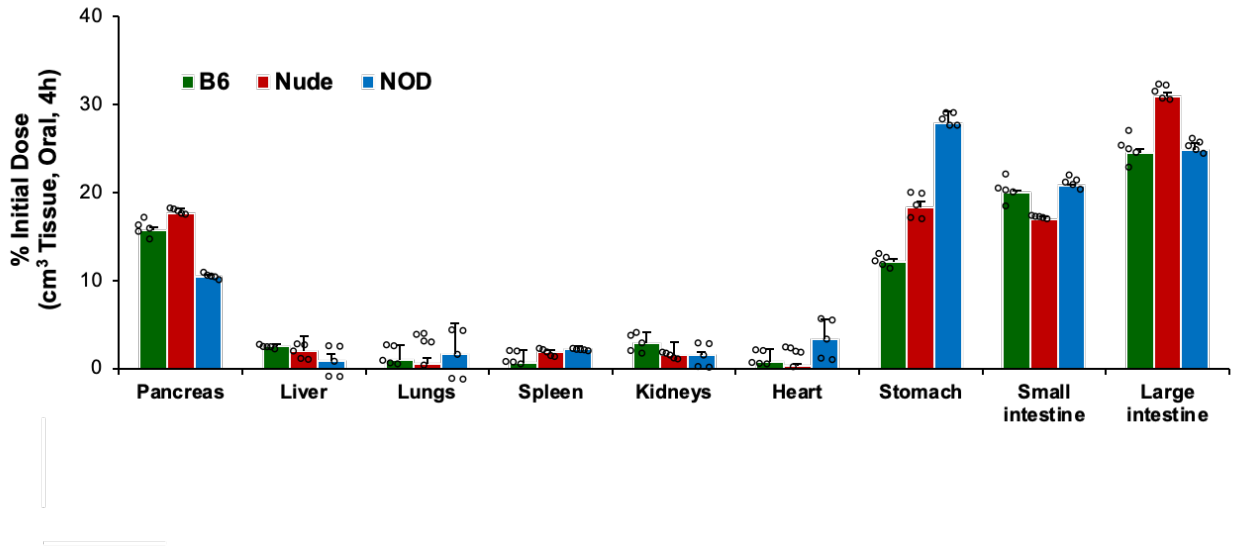

Supplementary Fig. 6. Mouse genetic independent biodistribution of pUDCA NPs. C57BL/6 mice (B6), Nude, and NOD mice were treated with DIR-pUDCA NPs by oral gavage (500 mg/kg) (n=5, mean ± SD). Mice were sacrificed at time points of 4 h post gavage and organs were harvested to measure the particle uptake. High particle accumulation in the pancreas was verified in different mouse strains and it was not a strict function of mouse genetics.

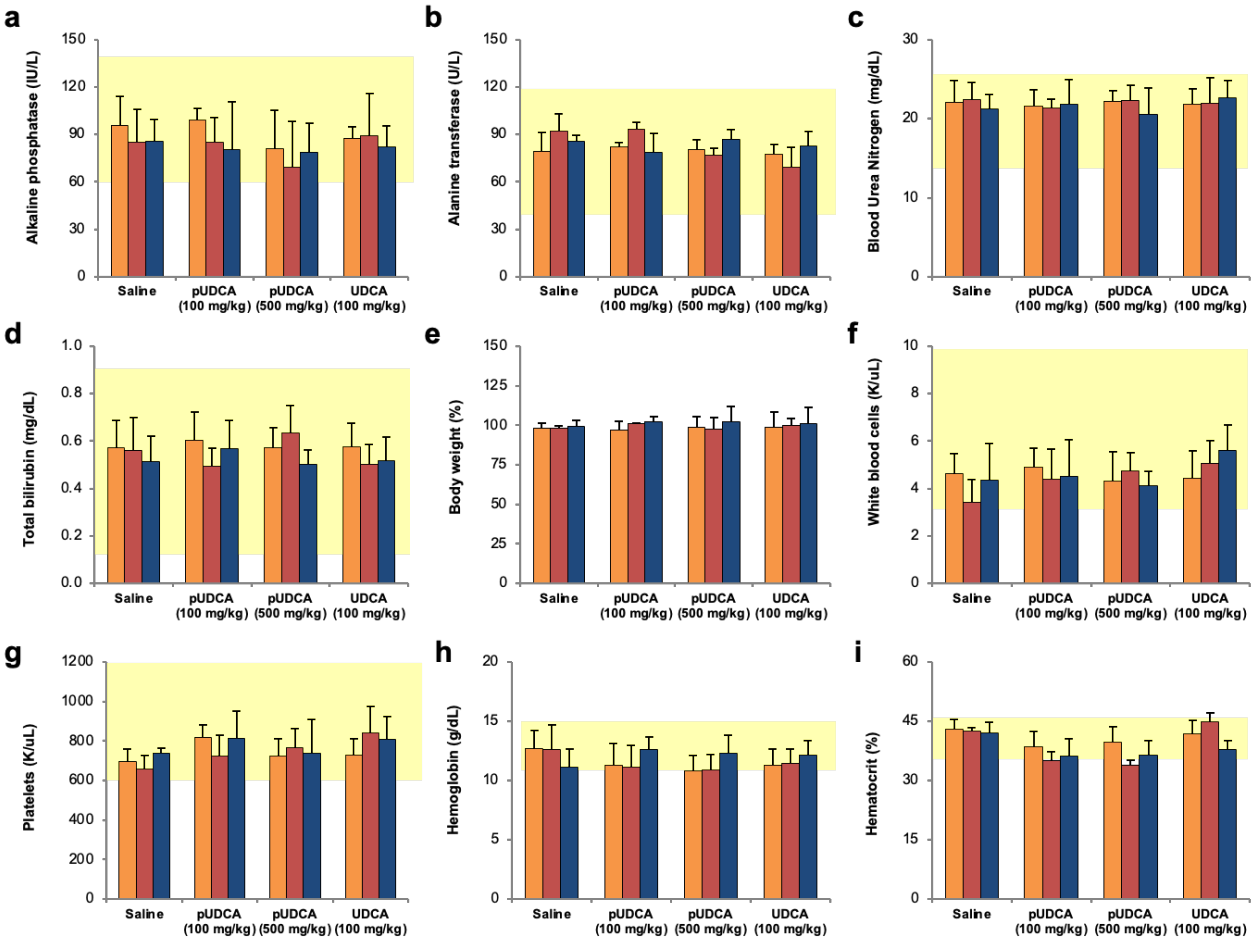

Supplementary Fig. 7. *In vivo* safety profile of pUDCA and UDCA after oral ingestion. Acute toxicity studies were performed in B6 mice (n=5, mean ± SD). Mice were orally dosed with pUDCA (100 and 500 mg/kg) and UDCA (100 mg/kg) at day 0. Serum concentrations of alkaline phosphatase, alanine transferase, total bilirubin, and blood urea nitrogen were measured using reagents from Teco Diagnostics at day 3 (orange bar), 5 (red bar), and 7 (blue bar) to compare with a saline group. Serum clinical chemistries were within normal physiological range (yellow region) for **a**, alkaline phosphatase (62-209 IU/L), **b**, alanine transferase (28-152 IU/L), **c**, total bilirubin (0.1-0.9 mg/dL), and **d**, blood urea nitrogen (18-29 mg/dL). No liver or renal toxicity was observed and **e**, body weight was normal. EDTA-treated blood was analyzed for hematotoxicity. Complete blood count (CBC) measurements were within the normal reference range (yellow area) for **f**, white blood cells (1.8 – 10.7 k/μL), **g**, platelets (592 – 2971 k/μL), **h**, hemoglobin (11.0 – 15.1 g/dL), and **i**, hematocrit (35.1 – 45.1 %).

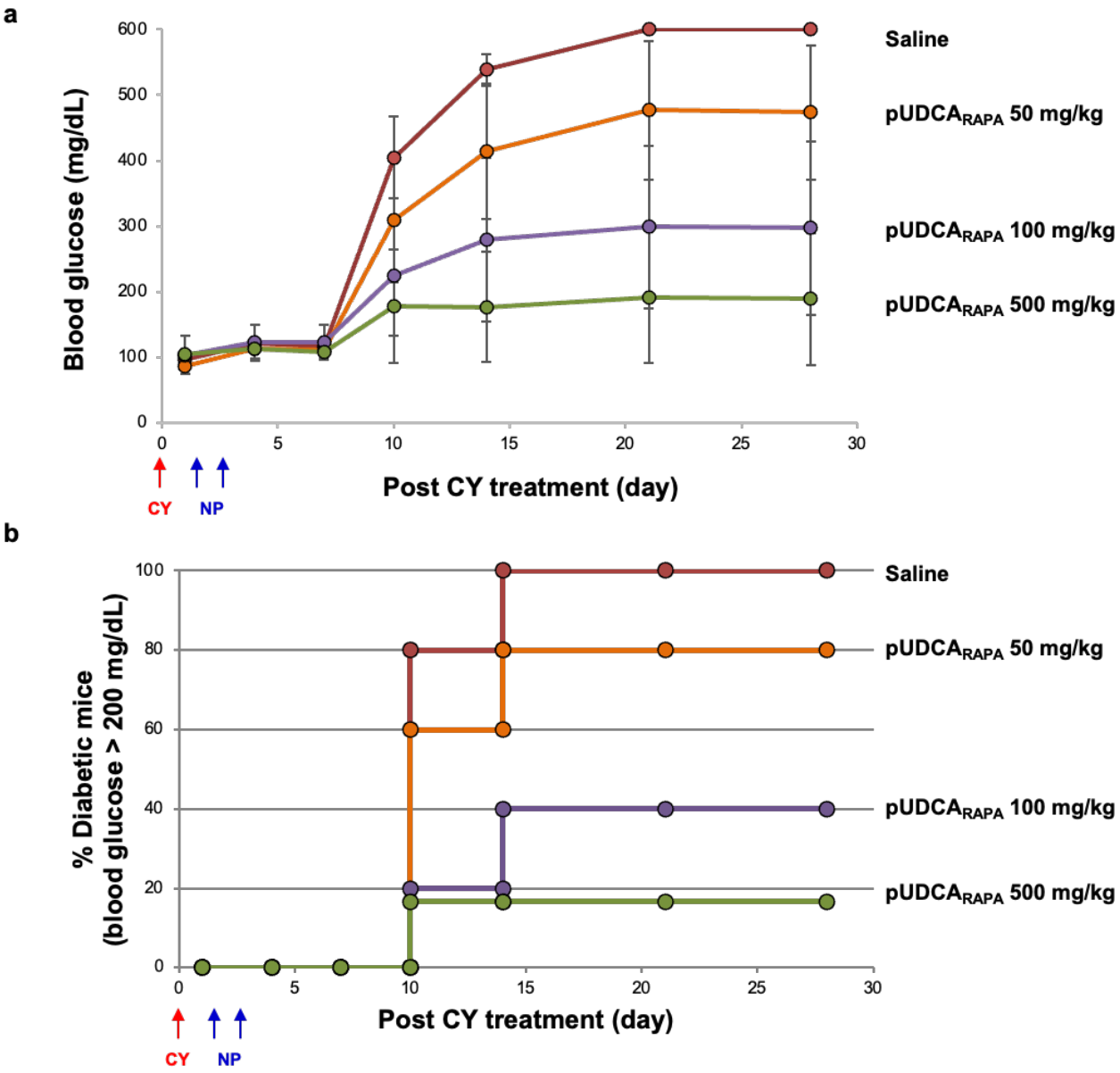

Supplementary Fig. 8. Dose-dependent therapeutic efficacy in prevention of T1D with rapamycin-loaded pUDCA NPs (pUDCA$_{RAPA}$). The prophylactic effect of Rapa-loaded pUDCA was tested as a function of dose in CY induced T1D animal models (n=5-6, mean ± SD). Doses were: 50, 100 and 500 mg/kg pUDCA. pUDCA was orally administered for two days (blue arrows) one day post CY induction (day 0, red arrow). The results indicate a prophylactic effect (i.e prevention of disease onset) that is dose-dependent as assessed by degree of **a**, blood glucose lowering and **b**, percentage of animals that were non-diabetic after 30 days. The indicator for diabetes onset was a blood glucose level greater than 200 mg/dL.

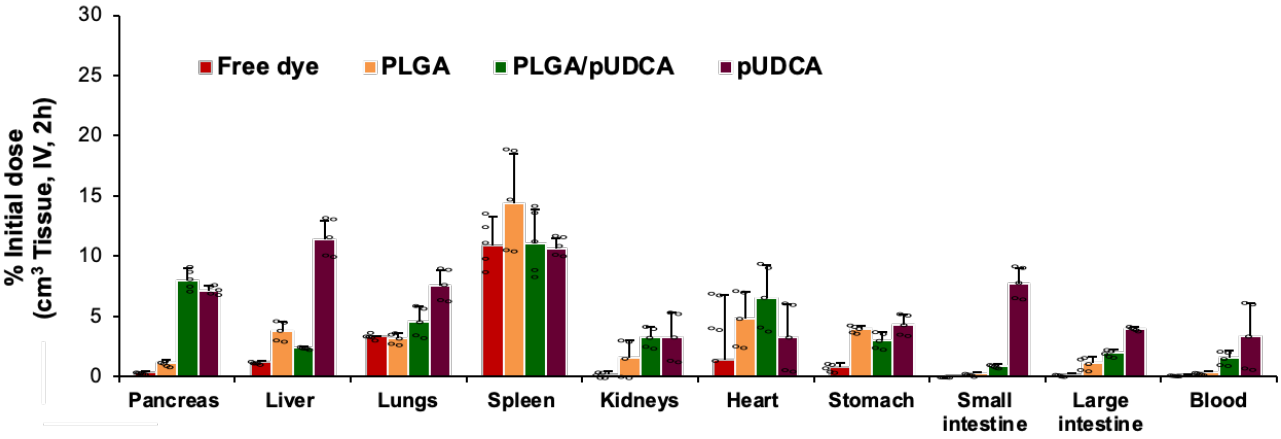

Supplementary Fig. 9. Biodistribution of pUDCA NPs after IV injection. To elucidate mechanism to pUDCA NP circulation, we intravenously (IV) injected the NP (n=5, mean ± SD). pUDCA, PLGA, and the blend NPs (100 mg/kg, 50 μL) were intravenously (IV) administered to B6 mice *via* tail vein and compare to free dye. Organs and blood were collected and measured at 2 h post ingestion. We observed high pancreatic accumulation of IV injected pUDCA NP, which was similar to the observations with orally gavaged pUDCA particles, indicating that pancreatic accumulation involved transport by macrophages cells and/or serum albumins, which are critical components governing biodistribution and clearance of foreign particles in the blood. Pancreatic accumulation thus was not entirely driven by enterohepatic circulation.

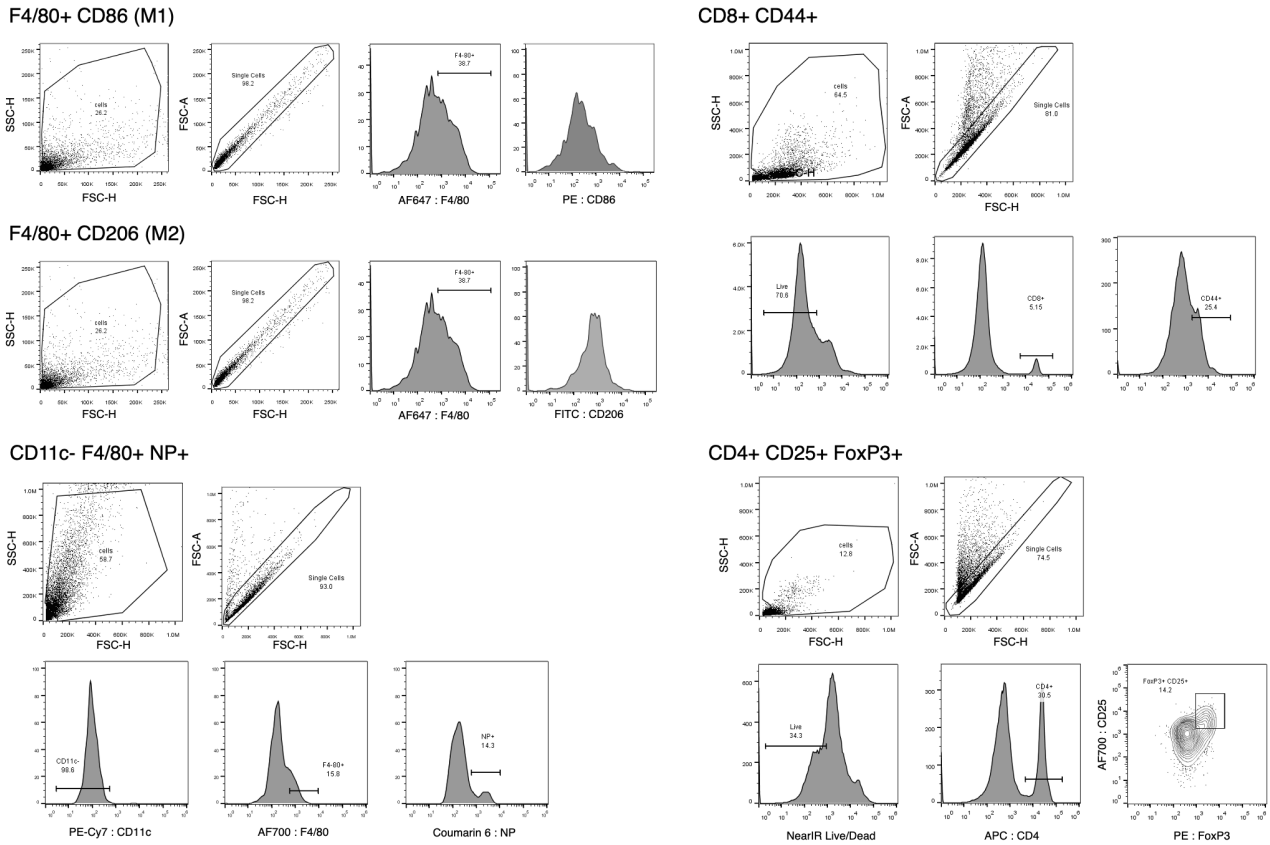

Supplementary Fig. 10. Flow Cytometry (FACS) Gating Strategies. Shown are the gating strategies utilized for analysis of M1 and M2 Macrophage phenotypes with and without the nanoparticle platform

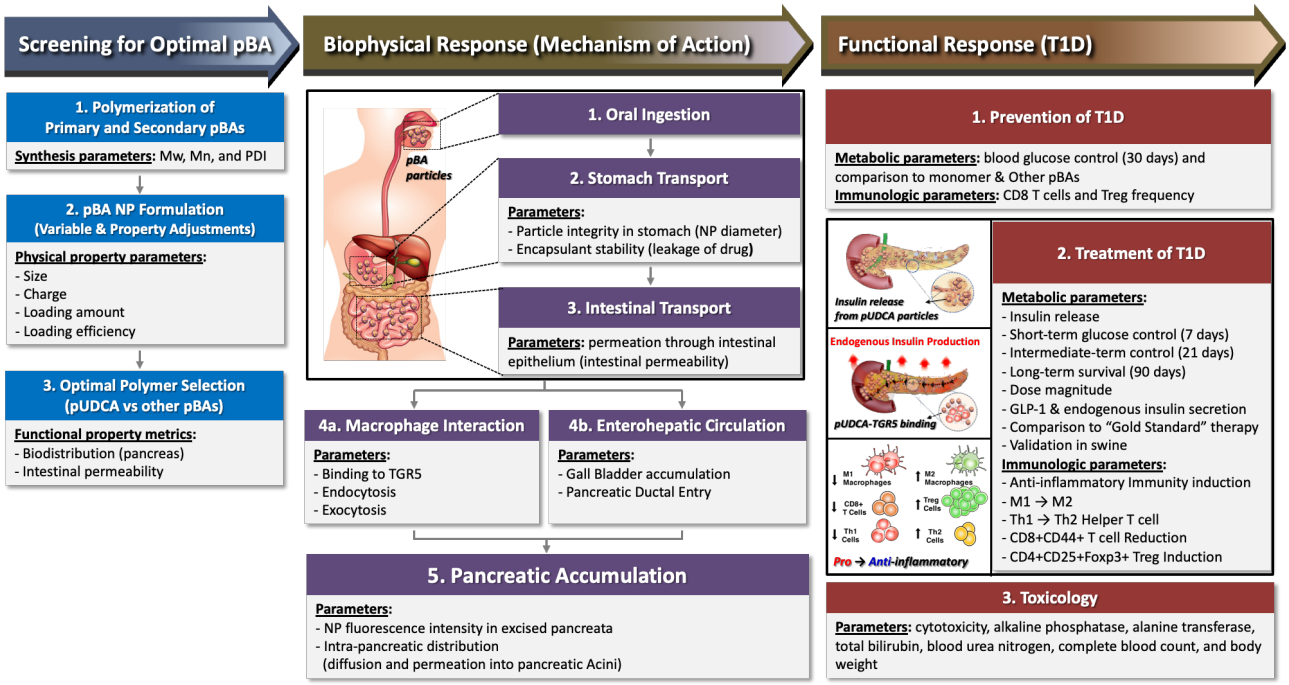

Supplementary Fig. 11 Design parameters and effects of polymerized bile acid NP: Summary. Attributes of the pUDCA platform responsible for the enhanced biotransport, restoration of metabolic control, and immunomodulatory mechanisms. After screening for optimal BA polymers, a comprehensive evaluation of biodistribution and mechanisms responsible for biodistribution were elucidated. The functional response resulting from such mechanistic improvements is shown in the last column which describes the prevention and treatment of T1D studies along with an investigation of the toxicology of pBA NPs.